Adiabatic stabilization: Observation of the surviving population

N. J. van Druten,* R. C. Constantinescu, J. M. Schins,† H. Nieuwenhuize, and H. G. Muller
FOM–Institute for Atomic and Molecular Physics, Kruislaan 407, 1098 SJ Amsterdam, The Netherlands
(Received 27 August 1996)

Photoionization of the circular $5g$ Rydberg state in neon by an intense subpicosecond light pulse is studied. Both the photoionization yield and the remaining population are measured. We find that the photoionization yield does not increase when the pulse peak intensity is increased above 60 TW/cm^2, and that a large fraction of the population remains in the $5g$ state instead. These results are consistent with predictions for adiabatic stabilization. The measurements are done using a sequence of three laser pulses. The first laser pulse excites the circular $5g$ state from the neon ground state, the second pulse is the intense light pulse that leads to the ionization (or lack thereof due to stabilization) we actually study, and the third pulse is a low-intensity high-fluence pulse ionizing all of the remaining $5g$ population. The photoionization yields of these three pulses are detected and separated by electron spectroscopy. [S1050-2947(97)04001-8]

PACS number(s): 32.80.Rm, 42.50.Hz

I. INTRODUCTION

The advent of intense light sources in the past decades has made it possible to study photoionization of atoms in situations where the light field is no longer a small perturbation. Theoretical investigations of such cases have led to the prediction of a number of interesting deviations from conventional perturbation theory (see Ref. [1] for a review of the theory of atoms in intense laser fields). One of the most spectacular of such deviations, first predicted by Pont and co-workers [2,3], is now known as *adiabatic stabilization*. It was found that for a sufficiently high-intensity, high-frequency field, the ionization rate *decreases* with increasing intensity. Subsequent calculations confirmed this effect [4–6], and showed that adiabatic stabilization can occur under experimentally realizable circumstances, if circular Rydberg states are used as initial states [7–9].

The first experimental evidence for this phenomenon was reported by de Boer *et al.* [10,11]. In these experiments the $5g$ circular Rydberg state in neon was prepared using a 1-ps, 286-nm wavelength, circularly polarized laser pulse, and the photoionization yield due to a second, 620-nm laser pulse of either 100-fs or 1-ps duration was studied. It was found that the ionization signal due to an intense (100-fs) pulse saturated in this experiment at a value significantly smaller than the initial population of the state. A lower limit for this latter population was determined from the ionization by a longer, less intense (1-ps) pulse. The fact that the photoionization yield due to these pulses *of the same fluence* differs, clearly demonstrates nonperturbative behavior, at an intensity where the calculations [9] predicted stabilization.

Since the experiment by de Boer *et al.* did not reveal the appearance of any new ionization signal in the electron spectrum from the short pulse as compared to the long pulse, it was concluded that the decrease of the single-photon ionization signal was due to population remaining behind in the $5g$ state, and thus strongly indicated stabilization of this state. To rigorously rule out alternative explanations, such as (Raman) transitions to long-lifetime states that could act as population traps, or ionization as some broad (and hence easily unnoticed) feature in the electron spectrum, we here extend the experimental study of the system used in Refs. [10,11]. We do this by not only measuring the photoionization yield from an intense laser pulse, but also the population that is left in the bound states after this pulse. The latter population is measured by adding a third, long low-intensity laser pulse arriving after the two light pulses mentioned above. This third laser pulse photoionizes all of the population remaining in the ng Rydberg states (amongst which the initial $5g$ state) after the second laser pulse, and the resulting photoelectrons (which are easily identified in the electron spectrum) are a measure for this population. Thus the present experiment shows extra evidence of, and gives more information on, the process of adiabatic stabilization.

It is worth noting that several other mechanisms of stabilization have been proposed in addition to adiabatic stabilization, that also would lead to suppression of the ionization signal (see, e.g., Ref. [12] for a comprehensive discussion). Some of those, such as transient [13] and interference [14] stabilization, specifically operate for manifolds of closely spaced levels, while others, such as channel closure due to Stark shifts [15] are more generally applicable. Since we performed our experiment on a Rydberg state, one might legitimately wonder why we interpret our results in terms of adiabatic stabilization only. Much information can be derived from our measured electron spectra other than merely the amount of ionization and remaining ground-state population, however. In Sec. V we will discuss how this information can be used to rule out other forms of stabilization.

In the following sections, we will give a brief summary of the theory of adiabatic stabilization, describe the experimental setup, and discuss the results of the experiments. The central result of this paper is shown in Fig. 8, and is discussed in Sec. IV C. In Fig. 8 it can be clearly seen that the Ne $5g$ state exhibits stabilization, strongly supporting the claim by de Boer *et al.*

*Present address: Huygens Laboratory, Leiden University, P.O. Box 9504, 2300 RA Leiden, The Netherlands.

†Present address: Department of Applied Optics, Twente University, P.O. Box 217, 7500 Enschede, The Netherlands.

II. THEORY

When a bound atomic state $|i\rangle$ is subjected to a light field, the light can usually be treated as a small perturbation. If the state can be one photon ionized by the light field, this results in the well-known Fermi's golden rule (FGR) [16]. The photoionization rate is then determined by the cross section σ, given by (in atomic units)

$$\sigma = 2\pi |\langle i|V|f\rangle|^2 \rho(E_f), \tag{1}$$

where V is the perturbation operator (r, for the case of an electric dipole transition, in the Coulomb gauge), and $\rho(E_f)$ is the density of final states $|f\rangle$ at the final-state energy E_f. The ionization rate is σI, where I is the intensity of the light. Since σ is independent of I, the final population p_f in $|i\rangle$ after a light pulse with fluence $F = \int dt\ I(t)$ is

$$p_f = e^{-\sigma F}, \tag{2}$$

where the initial population has been normalized to unity. Note that, according to FGR, the ionization yield does not depend on the details of the shape of the light pulse, but only on the total fluence contained in it.

Strong deviations from FGR can occur in a number of situations, e.g., when the pulse duration is shorter than the typical response time of the atomic state [13], when the coherence of several atomic initial states is important [14,17], in the presence of resonances [18,19], when the final-state continuum has structure (e.g. an autoionizing state) [20], or when multiphoton transitions are important [21]. These nonperturbative effects all have in common that they are caused by a structure that was already present in the unperturbed atom. In contrast, the effect that is now known as adiabatic stabilization, which was first discussed by Pont *et al.* [2], deals with a complete restructuring of an atom by a strong, high-frequency light field. Although the actual calculation of the restructured atomic states requires significant computational power, the physical mechanisms behind this effect can be understood qualitatively fairly easily, as will now be discussed (see also Ref. [22]).

A free electron in a light field will be driven in an oscillatory motion by the electric-field component of the light (neglecting relativistic effects, in which the magnetic-field component becomes important as well). The amplitude α_0 of this quiver motion is given, in atomic units, by $\alpha_0 = \omega^{-2}\sqrt{I}$, where ω is the frequency of the light.

The behavior of a bound electron will be very similar to that of a free electron if the oscillation period of the light is much shorter than the time scale on which the electron moves around in its orbit (the so called high-frequency condition). In other words, if the frequency of the light is high compared to the relevant energy in the atomic state, the electron will be driven in a rapid quiver motion, superimposed on the original orbit. For small oscillation amplitudes, this is only a weak perturbation of the atomic structure. The probability of an inelastic collision with the atomic core (leading to photoionization) increases with increasing quiver amplitude, in accordance with FGR.

For oscillation amplitudes that are much larger than the size of the initial (unperturbed) state, however, this is no longer true. As a result of the large quiver amplitude the average distance of the electron to the core will increase, and the time spent near the core will decrease. Thus the average force of the core on the electron will *decrease* with increasing light intensity. For a sufficiently large quiver amplitude, this results in a decreasing ionization yield as a function of laser intensity [3]. It can be incorporated into Eq. (1) as an ionization cross section that is a function of intensity I, decreasing more rapidly than $1/I$ above some critical intensity. This is the effect known as adiabatic stabilization, since when the intensity is increased from zero, the unperturbed atomic state adiabatically evolves to the strongly perturbed state at high intensities, which is again stable. Note that in this process, the decay rate $\sigma(I)I$ will go through a maximum [or, equivalently, the lifetime $1/\sigma(I)I$ will go through a minimum, known as ''Death Valley'' [10,11]]. Thus in an experiment, where the high intensities needed can only be reached in a pulsed laser field, the pulse rise time needs to be shorter than the minimum lifetime (i.e., in Death Valley), but at the same time sufficiently long so that nonadiabatic effects are negligible.

The original calculations were done for the ground state of atomic hydrogen. The above restrictions, however, require a light source far beyond current experimental possibilities in this case ($\hbar\omega \gg 13.6$ eV, $I > 10^{17}$ W/cm^2, pulse rise time < 10 fs). Subsequently [8,9], it was realized that the use of excited states could significantly relax these requirements, and a recent experiment [10,11] indeed showed evidence of adiabatic stabilization, for the circular $5g$ Rydberg state in neon, using an intense subpicosecond light pulse (linearly polarized). Due to its high angular momentum this state hardly penetrates the atomic core, and is nearly identical to the circular $5g$ state in atomic hydrogen, and the results of the experiments agreed with calculations on this state in hydrogen [9]. The motivation for the choice of this particular state was discussed extensively in Ref. [11]. We only summarize the general advantages of circular Rydberg states here.

Due to the weak binding energy ($1/2n^2$, for principal quantum number n) the high-frequency condition is already met at optical frequencies. More importantly, for the proper orientation of the quantization axis of the state (along the polarization direction of the light) no lower-energy states are accessible by electric dipole transitions. The circular Rydberg state has $m = l = n - 1$, where l is the quantum number of the orbital angular momentum, and m its projection along the quantization axis. This is the lowest-energy state with that particular m, and the linearly polarized light only causes transitions with the selection rule $\Delta m = 0$, so that only higher-energy states are coupled, and the high-frequency condition will remain satisfied. Furthermore, circular Rydberg states have very low probability density near the core, so that their perturbative photoionization cross sections are quite low, which is favorable for an increased minimum life time (in Death Valley). Thus it is possible to reach the stabilization regime with a reasonable pulse rise time (100 fs).

Finally, since photoionization at optical frequencies takes place within a range of ≈ 6 a.u. of the core [23], and the circular Rydberg-state wave functions have a small spatial extent in the polarization direction, especially near the core, quiver amplitudes of a few atomic units will already decrease the electron density there, reducing the ionization rate.

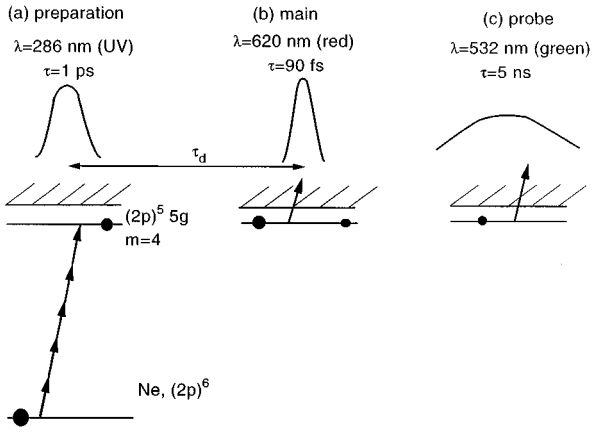

FIG. 1. Schematical representation of the laser pulse sequence used in the experiments. (a) The preparation pulse, a tightly focused UV laser pulse, excites the ground-state Ne atoms to the $5g$ Rydberg state. (b) The main pulse, an ultrashort intense laser pulse, applied with a variable delay τ_d ionizes part of the $5g$ population. (c) The probe pulse, a weakly focused, low-intensity laser pulse ionizes all of the $5g$ population surviving the intense main laser pulse. The photoionization signals resulting from pulses (a)–(c) are measured and separated using electron spectroscopy.

III. EXPERIMENTAL SETUP

The experimental setup is very similar to that described extensively in Ref. [11]. As mentioned in Sec. I, the experiment entails a sequence of three laser pulses, schematically depicted in Fig. 1. The three laser beams are collinearly overlapped in space, and focused in a standard magnetic-bottle electron spectrometer [24] filled with neon gas. We first describe the pulse sequence and its purpose, and then discuss the laser system used to generate the laser pulses.

The ''preparation'' pulse, of tightly focused circularly polarized ultraviolet (UV) light (wavelength $\lambda=286$ nm, pulse duration $\tau=1$ ps, $I\approx 200$ TW/cm^2), excites the ground-state Ne$(2p^6)(J=0)$ atoms by five-photon excitation to the $(2p^5)5g$ Rydberg state. This state is best described in jK coupling, as discussed extensively in Ref. [11]. Due to the $\Delta m=+1$ selection rule for photoabsorption of circularly polarized light, the final state has $m_J=5$, and the outer electron is dominantly excited from an initial $2p(m_l=-1)$ orbital to a circular $5g(m_l=l=4)$ orbital, where J is the total angular momentum, l is the orbital angular momentum of the electron, and m is the magnetic quantum number along the direction of propagation of the preparation pulse. The maximum admixture of other $5g$ components ($m_l=3$) is only 13% [11].

The second, ''main'' laser pulse, driving the ionization process that exhibits the stabilization, is an ultrashort ($\tau=90$ fs), linearly polarized, intense ($I\approx 100$ TW/cm^2) pulse of red light ($\lambda=620$ nm). The focus of the main pulse is chosen much larger than the focus of the preparation pulse, so that it completely envelops the prepared cloud of $5g$ states, and every atom in this cloud is subjected to main pulses with the same peak intensity. This circumvents the usual problem of averaging over focal intensities, that would make it next to impossible to recognize a saturating ionization signal amidst an increasing contribution from the low-intensity wings of the focus. The arrival time τ_d of the main pulse with respect to the preparation pulse is adjustable with subpicosecond precision (using an optical delay), and may be negative (corresponding to the main pulse arriving *before* the preparation pulse).

During the delay time the orientation of the $5g$ state will conveniently precess around the direction of the 0.9-T magnetic field in the electron spectrometer at the laser focus. This precession is used to align the angular-momentum axis of the circular state from its creation orientation pointing in the propagation direction, into a direction along the (electric-field) polarization vector of the main pulse, both of which are orthogonal to the magnetic field. In this way, the preparation and main pulse can be collinear, a necessary condition for the good focal overlap this experiment requires. After a quarter of the 80-ps precession period the rotation will be $\pi/2$ rad, and the $5g$ state will have predominantly $m_l=4$ character along a quantization axis parallel to the polarization direction of the main laser pulse, defining an optimum delay time of 20 ps for observing stabilization [11].

Finally, the third, ''probe'' laser pulse is a weakly focused, low-intensity green laser pulse (duration 5 ns, $I\leqslant 10$ GW/cm^2, $\lambda=532$ nm) delayed by 14 ns with respect to the preparation pulse, with a sufficiently high fluence to ionize all the $5g$ population (as well as population from neighboring states) surviving the main laser pulse. The photoelectrons resulting from these three laser pulses are collected over a 2π-sr solid angle by the diverging magnetic field [24], detected after a 0.5-m flight length by a multichannel plate detector, and energy analyzed according to their time of flight.

The laser system used to generate these three light pulses is very similar to the one described in Ref. [11] (see also Ref. [25]). In short, the $\lambda=620$-nm output of a colliding-pulse, mode-locked dye laser is amplified at 10 Hz in a chain of four Bethune-type dye cells, pumped by the second-harmonic output of a seeded Nd:YAG (yttrium aluminum garnet) laser. The dispersion in the dye cells is compensated using a folded prism compressor, resulting in a light pulse with a measured pulse duration of 90-fs full width at half maximum (FWHM), and an energy of ≈ 200 μJ.

A small fraction (20%) of this light is used as a seed from which eventually the UV preparation pulse is generated: it is focused in a water cell, creating a continuum of light throughout the visible part of the spectrum. Using a pulse shaper [25], a 3-nm bandwidth part of this light around $\lambda=572$ nm is selected, and is amplified to ≈ 1 mJ in a second chain of four dye cells. The spatial-mode quality of this beam is such that 50% of the light passes through a pinhole the size of the first dark ring of a diffraction-limited beam of the same size. This light is frequency-doubled in a 4-mm-thick potassium dihydrogen phosphate crystal and separated from the fundamental frequency by two dichroic mirrors to obtain ≈ 100 μJ of (linearly polarized) $\lambda=286$-nm light with a pulse duration of 1 ps.

The red light for the main pulse was obtained by spatially filtering the remaining 80% of the red light after the prism compressor, and sending it through an adjustable optical delay line before overlapping it with the UV beam. The energy in the red laser beam entering the spectrometer was varied by inserting apertures into the beam *before* the spatial filter. It was verified that this had no significant effect on the beam

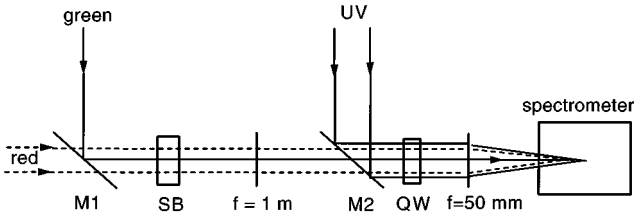

FIG. 2. Experimental geometry used to overlap and focus the three laser beams used in the experiments, and to ensure circular and linear polarization for the UV (preparation) and red (main) laser pulses, respectively. Mirror $M1$ was a high-power laser mirror, consisting of a glass substrate with a dielectric coating for maximum reflectance of 532-nm wavelength light at 45°, and was angle tuned for maximum transmittance of the red light. Mirror $M2$ was a harmonic separator, with a highly reflective coating for the UV, and excellent transmittance in the visible. QW denotes the quarter-wave plate for the UV, SB is the Soleil-Babinet compensator. See text for further details.

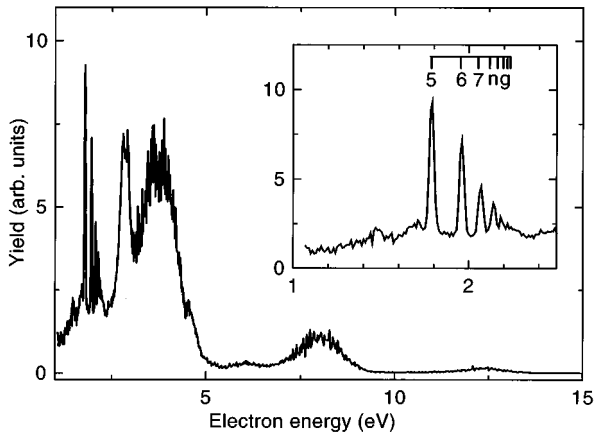

FIG. 3. Photoelectron spectrum obtained when the preparation (UV) and probe (green) laser pulses are applied. The inset shows part of the spectrum on an enlarged horizontal scale. The population of ng states, created by the preparation pulse, shows up in the peaks near 2 eV due to ionization by the probe pulse. The expected positions for these peaks are also indicated.

profile after the spatial filter. Note that, contrary to Ref. [11], no frequency selection or reamplification was applied to the red beam after the spatial filter. The green probe light pulse was derived from the same seeded Nd:YAG laser as was used for pumping the amplifying dye cells.

The energy of the main (red) laser pulse was measured on a shot-to-shot basis by a photodiode, and the electron spectra were collected into several intensity bins on the basis of this signal. For the study of the production of $5g$ population (i.e., in the absence of the main pulse; see Sec. IV A), the energy of the preparation (UV) pulse was measured instead, using the same procedure.

The geometry used to overlap the three beams spatially and focus them into the spectrometer is shown in Fig. 2. As in Ref. [11], the lens with a focal length of 1 m in Fig. 2 was used to compensate for the chromatic aberration of the final lens (50-mm focal length) focusing all beams in the spectrometer, in such a way that the longitudinal position of the red and UV foci overlapped. In addition it was used to fine tune the lateral position of the red and green foci with respect to the UV focus. The focus of the green light could also be moved independently from the position of the focus of the red light, by adjusting mirror $M1$. In this way the relative positions of the three foci could be controlled. The diameters of the three beams were set (using separate telescope lens combinations, not shown) such that the UV focus was smaller than the red focus, which was in turn smaller than the green focus (the focal sizes were verified *in situ*, see Sec. IV B).

The quarter-wave plate QW converts the polarization of the UV beam from linear to circular. Since mirror $M2$ was highly reflective only for the initial linear polarization direction of the UV, the quarter-wave plate had to be positioned after this mirror. The Soleil-Babinet compensator SB was set to obtain half-wave retardation for the red light for its combined action with the quarter-wave plate QW, rotating the linear polarization of the red light from horizontal to vertical (i.e., from parallel to perpendicular to the magnetic field in the electron spectrometer). Since mirror $M1$ only had good transmission for the horizontally polarized red light, the Soleil-Babinet compensator was positioned after this mirror. Mirror $M2$ had good polarization-independent transmission for both visible light beams. No effort was made to compensate for the effects of the polarization optics SB and QW on the polarization of the green light, since this polarization was irrelevant for our purposes.

IV. RESULTS

A. Production of $5g$ population

Before discussing the results obtained with the three-pulse sequence, we first discuss the production step of the $5g$ states. To optimize this production, we studied the electron spectrum for the case that only the preparation and the probe pulse are present.

An example of such a spectrum obtained in the present experiment is shown in Fig. 3, and is very similar to the one discussed in Ref. [11]. The spectrum is dominated by the photoelectrons due to the preparation light, consisting of a series of three broad peaks spaced by the UV-photon energy, corresponding to nonresonant six-, seven-, and eight-photon ionization. The nominal position expected for these peaks at the UV photon energy used (4.34 eV) would have been 4.45, 8.79, and 13.13 eV, respectively. The shift and broadening by about 1 eV of these peaks towards lower electron energies is due to the ac Stark shift of the ionization potential at the high intensities needed to drive the $5g$ excitation [11,26] (0.76 eV at 100 TW/cm^2). At zero field, five-photon ionization is also above threshold, but by such a small energy (0.11 eV) that this channel is closed by ponderomotive up-shift of the threshold before the intensity is high enough to drive it in any observable way.

From the shifts we estimate the peak intensity of the preparation pulse in Fig. 3 to be 200 TW/cm^2. The feature at 2.8 eV is not due to neon, but to a small H_2O contamination of our Ne source. The small continuous background in the electron spectrum is probably due to ionization of background impurities by a low-order process, occurring in the extended outer fringes of the preparation focus.

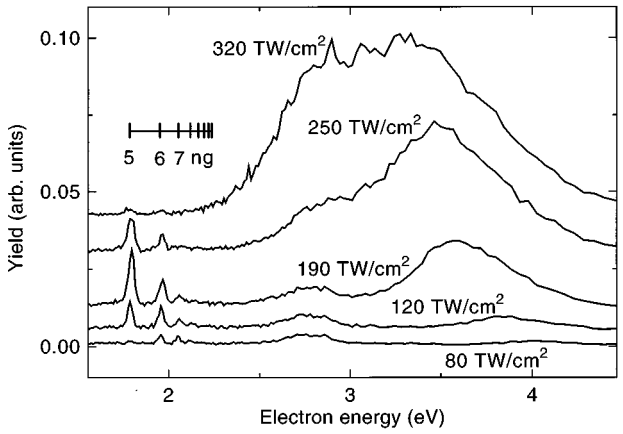

FIG. 4. Photoelectron spectra with both the preparation and probe pulses applied, for different peak intensities of the preparation pulse: 80 (lower trace), 120, 190, 250, and 320 TW/cm^2 (upper trace), respectively. The traces have been offset vertically for clarity. Note the intensity dependence of the strength of the peaks around 2 eV (due to the ng population produced by the preparation pulse and ionized by the probe pulse), and of the position and strength of the peak around 3.5–4.2 eV (due to six-photon ionization of Ne by the preparation pulse).

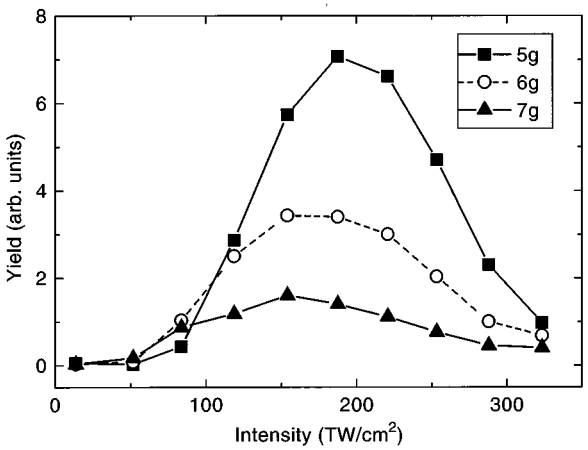

FIG. 5. Production of the $5g$, $6g$, and $7g$ Rydberg states as a function of peak intensity in the preparation pulse. The experimental data points are connected by lines to guide the eye. At the low-intensity side the production suddenly switches on as the state is shifted into resonance. At the high-intensity side the production tails off due to destruction of the Rydberg states by photoionization with the preparation pulse.

The large ac Stark shift of the ionization potential (mainly caused by the ponderomotive shift of the continuum threshold, the shift of the ground state being negligible) causes all members of the bound ng Rydberg series to shift through five-photon resonance with the ground state during the preparation pulse. Population is transferred to the Rydberg states during this process, and a large fraction of this population survives the preparation pulse due to the low ionization cross section of the g states [11,26]. This population can now be (single-photon) ionized by the subsequent probe pulse (photon energy 2.33 eV), and this gives rise to the narrow peaks around 2 eV shown on an enlarged scale in the inset of Fig. 3. The high energy resolution in this spectrum was obtained by adding several spectra with different retarding voltages, only using the high-resolution (long time of flight) part of each spectrum. The relatively long pulse duration of the probe pulse (5 ns) allows the combination of a large fluence with a low peak intensity, so that the g-state population is depleted by the probe pulse with negligible contribution from other (multiphoton) ionization processes and negligible Stark shifts. Varying the energy of the probe pulse by a factor of 2 did not change the photoionization yield from the g states, proving that this pulse completely depletes the population in these states.

It was exceedingly difficult to produce large $5g$ populations, and the optimization of this process was the key to success of the entire experiment. This optimization also involved tuning the focusing conditions. To this end, the production process was studied as a function of the preparation pulse intensity. Typical spectra used for these measurements are shown in Fig. 4, and the surface area of the Rydberg ionization peaks in these spectra is plotted in Fig. 5 as a function of preparation pulse intensity. The peaks can be seen to appear quite suddenly at the intensity for which the corresponding state is shifted into resonance, and it is also clear from the data that the higher states shift into resonance at the lowest intensities. A precise determination of the appearance of the various Rydberg ionization signals results in an accurate calibration of UV intensity.

A factor 2 above its appearance intensity, the $5g$ production already starts to decrease. This sensitivity of the Rydberg population with respect to the UV intensity is readily explained by the fairly narrow range of peak intensities for which appreciable $5g$ population can occur. A minimum intensity of 86 TW/cm^2 (a ponderomotive shift of 0.66 eV) is needed to shift the $5g$ state into five-photon resonance with the ground state. On the other hand the saturation fluence for photoionization of the $5g$ state by the UV pulse (395 J/cm^2 [11]) sets an upper limit to the intensity in the 1-ps UV pulse of about 400 TW/cm^2, above which the Rydberg population is destroyed by ionization. Thus high-UV intensities only cause unnecessarily large ionization by the preparation pulse, possibly reducing detection efficiency for the low-energy peaks arriving in the aftermath of this huge bulk of ionization. To prevent any corruption of the stabilization data by such an artifact, care was taken to perform all later runs with identical preparation conditions, as monitored from the magnitude and shape of the 3.5-eV ionization hump.

After the intensity at which optimum production occurred had been established, the focal volume was adjusted to reach this intensity at the maximum UV pulse energy, in order to have as large a production volume as possible. This was accomplished by slightly tuning the divergence of the $\lambda = 572$-nm beam before it entered the doubling crystal. Doing so affects the divergence of the UV beam exiting the crystal, and thus the size of the UV beam on the final focusing lens. This in turn determines the size of the UV focus in the spectrometer. The amount of $5g$ population created by the UV pulse was found to be very sensitive to this focusing geometry, because the focal volume grows with the fourth power of the focal radius. At the available UV energy of about 100 μJ, optimal production was achieved for a 4-mm-diameter UV beam at the final focusing lens. This corresponds to a minimum (diffraction-limited) focal size of 4 μm

for the UV, and a corresponding maximum peak intensity of 600 TW/cm^2. Allowing for the same reduction to 50% of this value as the fundamental due to the nonperfect mode quality, this agrees well with the intensity calibration based on the Stark shifts. The maximum population in the $5g$ state was thus found for the results shown in Fig. 3, i.e., for a peak intensity of 200 TW/cm^2, and for the optimum focusing geometry mentioned above.

B. Focus size determination

When the main pulse is added, the spectra of Fig. 6 result. These spectra were obtained at a single retarding voltage, hence the decreased energy resolution (compared to Fig. 3). The fluence of the main pulse at the UV preparation focus was 6 J/cm^2 in this case. Photoionization of the g states by the main pulse leads to a similar series of peaks in the photoelectron spectrum as in Fig. 3, but displaced down in energy by 0.33 eV, the energy difference between main (red) and probe (green) photons.

Clearly, for $\tau_d = 5$ ps [Fig. 6(a)], when the angular momentum of the $5g$ state is still pointing approximately in the propagation direction of the light, a substantial fraction of the $5g$ population is ionized by the main pulse, as can be seen both from the ''main'' photoionization peak at 1.45 eV, and from the strong decrease of the probe photoionization peak at 1.8 eV. For $\tau_d = 20$ ps [Fig. 6(b)], the angular momentum of the $5g$ state is parallel to the polarization direction of the main pulse, and photoionization is much reduced. By subtracting ''background'' spectra taken at $\tau_d = -5$ ps (also shown in Fig. 6) we can now accurately determine the strength of both the main and the probe photoionization peak [27].

We can use spectra like these for an *in situ* measurement of the focus size of the main pulse, and to verify the alignment of the laser foci, as shown in Fig. 7. In this figure, the $5g$-photoionization yields from the main and the probe laser pulse are shown (for $\tau_d = 5$ ps), as a function of the lateral position of the main and probe foci. Both foci were moved simultaneously by translating the prefocusing lens (focal length 1 m, see Fig. 2), as discussed in Sec. III. Since the size of the UV preparation focus is smaller than that of the main pulse focus, the $5g$ population created by the preparation pulse samples a small part of the main focus, approximately 4 μm, and the photoionization signal reflects the lateral focal shape of the main pulse at the longitudinal position of the preparation focus. Several of these scans were made for different longitudinal positions of the prefocusing lens, to determine experimentally the position for best longitudinal overlap of the preparation and the main pulse foci. Figure 7 shows the result for this position, for a horizontal scan of the lateral position of the prefocusing lens. A vertical scan looked very similar. From this we conclude a focus diameter for the main pulse of 10 μm (FWHM), consistent with diffraction-limited focusing.

The main pulse focus size can also be determined from the photoionization of the $5g$ state by the probe pulse, also shown in Fig. 7. Note that the decrease in this signal is approximately equal to the increase in the signal from the main pulse when scanning over the laser focus, providing additional experimental evidence that the probe pulse sufficiently

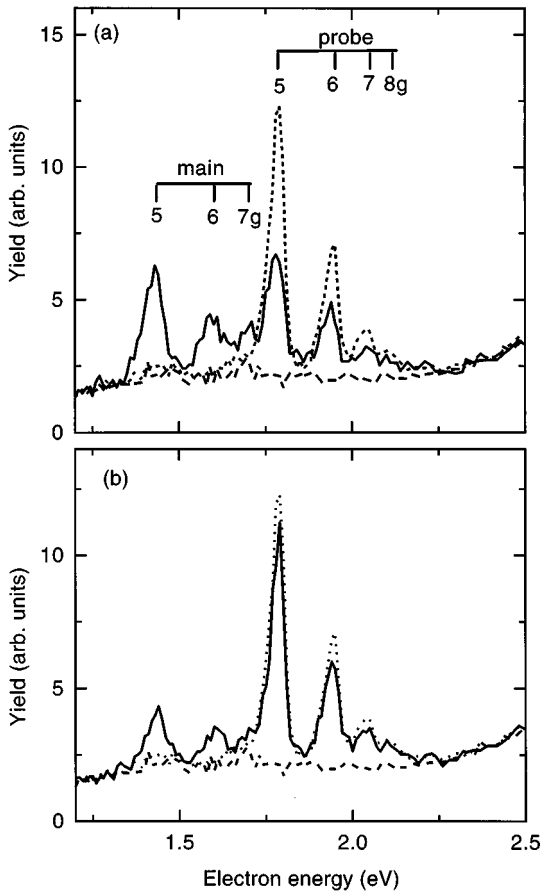

FIG. 6. Examples of photoelectron spectra when preparation, main and probe pulses are all present (solid lines), for a delay between preparation and main pulse τ_d of 5 ps in (a) and 20 ps in (b). For comparison the spectra for $\tau_d = -5$ ps without (dashed) and with (dotted) probe pulse (used for the determination of background signal and full $5g$ population, respectively) are also shown. The expected electron energies for one-photon ionization of the ng states by the main and probe pulse are indicated.

depletes the leftover $5g$ population. It is also clear from this plot that the size of the probe beam is considerably larger (at the preparation pulse focus). Only when the probe focus is moved away from the preparation focus considerably further than the main focus size does the probe photoionization yield start to decrease again from its maximum value due to loss of spatial overlap between preparation and probe pulse. The onset of this is visible in the rightmost points of Fig. 7.

C. Adiabatic stabilization

We can now use these three-pulse photoelectron spectra to measure the photoionization behavior of the $5g(m=4)$ state under conditions where we expect adiabatic stabilization by going to $\tau_d = 20$ ps. We measured photoelectron spectra for $\tau_d = 20$ ps and -5 ps as a function of the energy of the main laser pulse. The photoionization yields from the main and the probe pulses for $\tau_d = 20$ ps were normalized to the initial $5g$ population, as determined from the $\tau_d = -5$ ps spectra. The result is shown in Fig. 8. It is clear that the data show a strong deviation from the behavior expected on the basis of Fermi's golden rule. Above a critical peak intensity

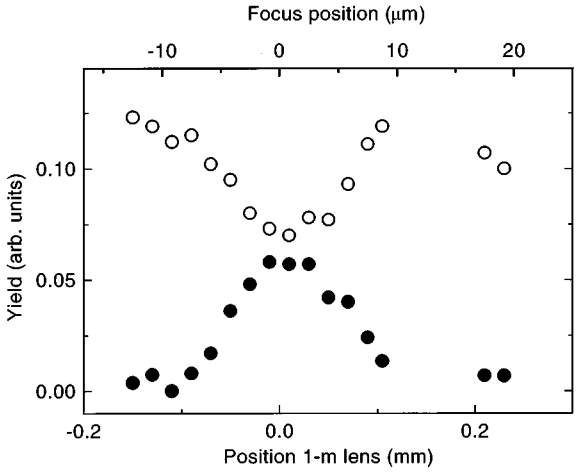

FIG. 7. Focus scan of the main pulse: photoionization yield from the $5g$ state by the main pulse (closed symbols) and the probe pulse (open symbols), as a function of the lateral position of the prefocusing lens.

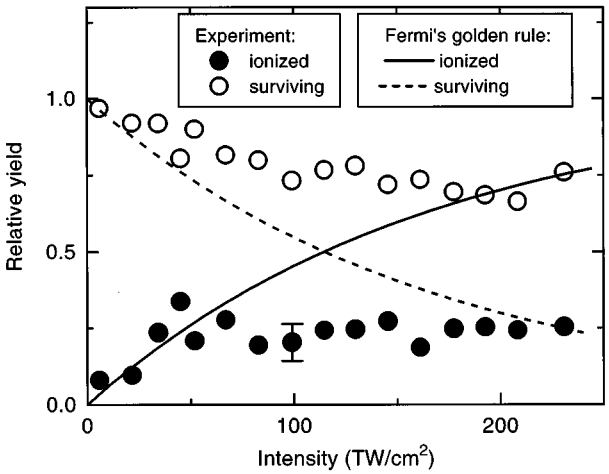

FIG. 8. Observation of adiabatic stabilization: measured ionized and surviving fraction of the $5g$ population (solid and open symbols respectively) in photoionization by the main pulse, as a function of main-pulse intensity. The theoretical curves based on Fermi's golden rule (FGR) for ionized and surviving fraction are also shown (solid and dotted line, respectively). The data clearly show a strong deviation from FGR, and a surviving fraction of 70%, even at the highest intensities. This is clear evidence of stabilization. The experimental fractions were determined from the three-pulse photoelectron spectra, as described in the text. The theoretical curves are based on the known (perturbative) ionization cross section of the $5g$ state [11]. The estimated size of the experimental error bars is indicated.

in the main pulse of ≈ 60 TW/cm^2 (corresponding to a fluence of 5 J/cm^2), hardly any additional ionization is observed when the peak intensity is increased to the maximum of $\approx$ 200 TW/cm^2. The (one-photon) ionization yield from the main pulse saturates at $\approx 25\%$ of the initial population. These observations are consistent with the previous measurements by de Boer *et al.* [10,11], and with theoretical predictions for adiabatic stabilization of the $5g(m=4)$ state at $\lambda = 620$ nm [9]. The above saturation value could not be determined directly in the previous measurements on adiabatic stabilization [10,11].

The present results also allow us to determine the fraction of the population that is left in the initial state. Figure 8 shows that a population fraction of $\approx 70\%$ survives in the initial state even at the highest fluences. Note that the complementarity of the two signals in Fig. 8 shows that no other decay channels than single-photon ionization are significant at the 10% level. These measurements thus provide strong additional evidence of the occurrence of adiabatic stabilization.

V. DISCUSSION AND CONCLUSION

The most important fact about the electron spectra of Fig. 6 is that the ionization signal out of the Rydberg states caused by the main pulse comes out in a narrow peak at its expected spectroscopic position one red photon above the Rydberg state. Because the magnitude of this peak is equal to the decrease of the probe ionization of the same state, no other (e.g. shifted or broadened) ionization signal from these states is present. The narrowness of the peak shows that the ac Stark shift of the Rydberg states follows the ponderomotive shift of the continuum to within 50 meV, at least up to the highest intensity contributing to the ionization (i.e., 60 TW/cm^2, corresponding to a ponderomotive shift of 2.16 eV). The $5g$ ionization peak thus remains at least 1.45 eV above threshold, and channel closure can be ruled out as a mechanism for shutting off the ionization.

Interference stabilization [14] leads to a characteristic jump of the Rydberg ionization signal to positions intermediate to the spectroscopic values at intensities above the rate minimum. The absence of such intermediate peaks thus rules out that the observed effect is interference stabilization. This is not surprising, since interference stabilization is expected to occur when the lifetime broadening of the peaks becomes comparable to their spacing, so that their ionization signals start to overlap and can interfere destructively. No hint of such lifetime broadening is observed in the electron spectra.

Transient stabilization [13], finally, is expected when the bandwidth of the ionizing radiation becomes larger than the level spacing, so that the laser can redistribute the initial population over a number of nearby states to set up a superposition of states whose ionization signals interfere destructively. This is not the case in the current experiment ($\hbar\Delta\omega \approx 8$ meV, $E_{5g} - E_{6g} = 166$ meV), and no redistribution of population between Rydberg levels is observed.

The neighboring members of the Rydberg series seem thus in no way involved in the ionization process, and the observed resistance of the remaining 70% of the population of prepared $5g$ Rydberg states to ionization above 60 TW/cm^2 must be due to adiabatic stabilization, just as the theoretical calculations predicted.

ACKNOWLEDGMENTS

This work is part of the research program of the ''Stichting voor Fundamenteel Onderzoek der Materie (FOM),'' and was made possible by financial support of the ''Nederlandse Organisatie voor Wetenschappelijk Onderzoek (NWO).''

[1] K. Burnett, V. C. Reed, and P. L. Knight, J. Phys. B **26**, 561 (1993).
[2] M. Pont, N. R. Walet, M. Gavrila, and C. W. McCurdy, Phys. Rev. Lett. **61**, 939 (1988).
[3] M. Pont and M. Gavrila, Phys. Rev. Lett. **65**, 2362 (1990).
[4] P. Marte and P. Zoller, Phys. Rev. A **43**, 1512 (1991).
[5] M. Dörr, R. M. Potvliege, D. Proulx, and R. Shakeshaft, Phys. Rev. A **43**, 3729 (1991).
[6] K. C. Kulander, K. J. Schafer, and J. L. Krause, Phys. Rev. Lett. **66**, 2601 (1991).
[7] M. Pont and R. Shakeshaft, Phys. Rev. A **44**, R4110 (1991).
[8] R. J. Vos and M. Gavrila, Phys. Rev. Lett. **68**, 170 (1992).
[9] R. M. Potvliege and P. H. G. Smith, Phys. Rev. A **48**, R46 (1993).
[10] M. P. de Boer *et al.*, Phys. Rev. Lett. **71**, 3263 (1993).
[11] M. P. de Boer *et al.*, Phys. Rev. A **50**, 4085 (1994).
[12] H. G. Muller, in *Physics with Multiply Charged Ions*, edited by D. Liesen (Plenum, New York, 1995), p. 239.
[13] J. H. Hoogenraad, R. B. Vrijen, and L. D. Noordam, Phys. Rev. A **50**, 4133 (1994).
[14] M. V. Fedorov and A. M. Movsesian, J. Opt. Soc. Am. B **6**, 928 (1989).
[15] H. Reiss, J. Phys. B **20**, L97 (1987).
[16] H. A. Bethe and R. Jackiw, *Intermediate Quantum Mechanics*, 3rd ed. (Addison-Wesley, Reading, MA, 1986).
[17] R. R. Jones, C. S. Raman, D. W. Schumacher, and P. H. Bucksbaum, Phys. Rev. Lett. **71**, 2575 (1993).
[18] Y. L. Shao *et al.*, Phys. Rev. Lett. **67**, 3669 (1991).
[19] S. Cavalieri, F. S. Pavone, and M. Matera, Phys. Rev. Lett. **67**, 3673 (1991).
[20] O. Latinne *et al.*, Phys. Rev. Lett. **74**, 46 (1995).
[21] J. H. Hoogenraad *et al.*, Phys. Rev. Lett. **75**, 4579 (1995).
[22] M. Gavrila, in *Atoms in Intense Laser Fields*, edited by M. Gavrila (Academic, San Diego, 1992), pp. 435–510.
[23] H. G. Muller and H. B. van Linden van den Heuvell, Laser Phys. **3**, 694 (1993).
[24] P. Kruit and F. H. Read, J. Phys. E **16**, 313 (1983).
[25] L. D. Noordam *et al.*, Opt. Commun. **85**, 331 (1991).
[26] M. P. de Boer, L. D. Noordam, and H. G. Muller, Phys. Rev. A **47**, R45 (1993).
[27] Note that we assume here that the red laser pulse does not deplete the ground-state Ne atoms, since this would cause a reduced $5g$ production by the UV pulse. This was justified up to the highest intensities used here.